Role of channel temperature and mass window in the binary breakup of ^{236}U*

C. Kokila and M. Balasubramaniam ⓘ*

Department of Physics, Bharathiar University, Coimbatore 641046, India

The dynamical cluster-decay model (DCM), an extension of the preformed cluster model of Gupta and collaborators for the decay of hot and rotating compound nuclei (CN) formed in low-energy reactions, has been applied to study the mass distribution of ^{236}U* formed at an excitation energy corresponding to the capture of thermal neutrons by ^{235}U. The role of excitation energy of the compound nucleus, neck length parameter, and mass window (range of mass numbers) considered are also analyzed. The excitation energy of the compound nucleus is kept fixed for all channels, and the temperature for each channel is obtained iteratively to conserve the sum of excitation energies of two fragments to the excitation energy of the compound nucleus at a fixed distance, mimicking the saddle configuration. The obtained mass distributions and yields are compared with experimental yields.

I. INTRODUCTION

There has always been a great interest in the study of fission yields since they are useful in understanding the nature of the fission process. Hence, the study of the mass distribution and charge distribution of the nuclear fission process is important. Since a large collective motion is involved in the fission process, starting from a parent nucleus to resulting fission fragments through deformation space, its description poses a challenge for any model or theory. In addition to the deformation degree of freedom, any model has to account for the experimental observables like mass distribution, kinetic energies of the fragments, etc. The data on low-energy nuclear fission studies have general implications for the understanding of the influence of shell structure on nuclear dynamics and the viscosity of cold nuclear matter. The observables from low-energy fission indicate the importance of microscopic features such as shell effects and pairing effects. Hence, a complete model must take into account the initial reaction that induced the fission process, the formation of the pre-compound nucleus, and the competition of particle emission, γ emission, and fission. The evolution of the fissioning system needs to be fully described, considering all degrees of freedom.

Many attempts have been made to develop methods for describing the fission-fragment yields and other fission properties. The description of fission observables relies on the modeling of the dynamics of the fissioning system. Many theoretical models have tried to account for the mass and charge distributions, average kinetic energy, excitation energy, and cross section, from fission fragments in the actinide fissioning system like ^{235}U(n, f).

Recently, in Ref. [1], the Langevin dynamical approach combined with a Monte Carlo method was used to study

the fission-fragment mass distribution, neutron and γ-ray multiplicity, and the average kinetic energy of an emitted neutron at a low excitation energy of the induced fission process of ^{236}U at $E^* = 20$ MeV. Further, by comparing the distribution with experimental data, they evaluated the timescale of fission. The Monte Carlo approach was used to calculate the evaporation of particles from fission fragments for thermal neutron-induced fission of ^{235}U and ^{239}Pu and for the spontaneous fission of ^{252}Cf in [2]. The decay of fission fragments from ^{235}U(n, f) was simulated by assuming that particles are only emitted from the fully accelerated fission fragments. The pre-neutron-emission fragment yield matrix is used to sample the total kinetic energy directly and the mass of the heavy fragment and then to determine the charge, spin, and parity of fission fragments.

In Ref. [3], Pasca *et al.* studied the shape of charge and mass distributions of the fission fragments for ^{235}U(n, f) and ^{239}Pu(n, f) with increasing incident neutron energy from the thermal energy up to 55 MeV using the statistical method of a dinuclear system model (DNS). Here, statistical equilibrium is assumed to be established at scission, and observable characteristics of fission processes are also assumed to be formed near the prescission configuration of the fissioning nucleus. Using a deformation, mass (charge) asymmetry dependent potential energy, they have calculated mass and charge distributions, total kinetic energy, and neutron multiplicity. With increasing incident neutron energy, the mass yields (charge yields) showed a decrease of asymmetric peak and an increase of fission yields in the near-symmetric mass (charge) region. They concluded that the washing of shell effects with an increase in excitation energy might be the cause for the change in mass and charge distributions.

In Ref. [4] Romano *et al.* measured the change of fission-fragment mass distribution of ^{235}U as a function of incident neutron energy. In this experiment, the neutrons are created in a (γ, n) reaction and are slowed down by successive

---

*m.balou@gmail.com

scattering collisions in the lead. The neutron energy is used to determine energy-dependent, neutron-induced fission cross sections as a function of neutron slowing-down time. Change of total kinetic energy (TKE) of the fission fragments is also examined and the TKE was found to increase with an increase in incident neutron energy. In Ref. [5], Paradela *et al.* measured the cross-section ratio of $^{238}U(n, f)/^{235}U(n, f)$ at the n_TOF facility at CERN from 0.5 MeV to 1 GeV. They have compared the cross-section ratio for neutron energies from 500 keV to 20 MeV with the data from ENDF/B-VII.1 [6,7].

In Ref. [8], Yanez *et al.* measured the total kinetic energy release in the neutron-induced fission of ^{235}U for neutron energies from 3.2 to 50 MeV. A decrease in total kinetic energy was observed with increasing neutron energy, which reflected the increase in symmetric fission with an increase in excitation energy. Further, their results are compared with the predictions from the GEF model (GEneral description of Fission observables) [9]. Yanez *et al.* in [10] measured the total kinetic energy release in the fast neutron-induced fission of ^{235}U in the neutron energies from 2 to 100 MeV. The spallation neutrons from a tungsten target were made to collide on a ^{235}U target, to detect the fission products using photodiodes. They found that the mean total kinetic energy values decrease nonlinearly with increasing neutron energy. Further, the measured total kinetic energy distributions are compared with the results from the GEF model [11]. In addition, many experiments were performed to determine the total γ-ray emission from neutron-induced fission of ^{235}U [12–14]. The GEF model applies to all fissioning systems from spontaneous fission up to excitation energies of 100 MeV. The model is suitable for large-scale calculations. In this model, properties like fission mode, mass division, fragment excitation energy, total kinetic energy were determined. A global fit procedure is done on the ingredients of the model and its parameter values, hence the deviations from the experimental values are found to be minimum.

Recently, a new statistical scission-point model, called SPY [15] was developed to evaluate the mass distributions and mean values of all fission observables based on the Wilkins model [16]. In this model, scission-point distance is the only parameter. The model is based on the assumption that the gross properties of fission fragments depend on the available energy at the scission point. Statistical treatment is applied assuming thermodynamic equilibrium at scission. The scission configuration is characterized by neutron, proton, and deformation parameters of fragments and their separation distance. The potential energy, calculated within Hartree-Fock-Bogoliubov (HFB) formalism, was used to evaluate fission observables in the thermal fission of ^{235}U. A satisfactory reproduction was obtained for the total kinetic energy and mass yields. Taking clues from SPY model and the Wilkins model, one of us recently reported ternary fission mass distributions [17].

In Ref. [18], the static aspects of induced fission is studied in terms of a microscopic theory as a function of the excitation energy of the incident neutron. In this work, the excited states are described by random phase approximation or the generator coordinate method. Schunck *et al.* have studied the evolution

of fission barriers by assuming the potential energy surface (PES) of the compound nucleus in the HFB approximation. They have analyzed the influence of incident neutron energy on the fission barriers of the compound nucleus ^{240}Pu. In Ref. [19], the time evolution of ^{240}Pu is studied using the time-dependent density functional theory. Using the Skyrme parametrization, the structure of the nuclear energy density functional is obtained. The dynamics of the fission process is given by simulations from which the relative shape evolution could be understood.

With the collective wave function as the only input, the Gaussian overlap approximation of the time-dependent generator coordinate method (TDGCM-GOA) is used to study the dynamics of ^{238}U in Ref. [20]. In this work, the low-energy fission-fragment distributions, density plots, pairing energy, total kinetic energy, and mass distributions are studied. In Ref. [21], the TDGCM-GOA is used to investigate the transition from asymmetric to symmetric fission in neutron-rich fermium isotopes along with the Gaussian overlap approximation. In TDGCM-GOA, the many-body quantum state is determined by a variational approximation of the many-body dynamics. Potential energy landscapes, fission-fragment distributions, and primary-fragment charge yields are obtained for various fermium isotopes. It was observed that with an increase in neutron number, the symmetric mode dominates. Further, the role of initial state or energy of the fissioning system is studied using the Gogny interaction by assuming ground-state deformation.

Using the Fourier decomposition of nuclear shape, nuclear deformation-energy landscapes were investigated for pre-actinides and actinides ($78 \leqslant Z \leqslant 94$) in [22]. Here, the deformation properties of the nuclei, including the deformation energy, fission barrier height, Q value of α decay, α-decay half-lives, most probable fission path, etc., were studied in a four-dimensional deformation space of collective coordinates. Nuclear shape evolution in terms of a Metropolis walk treatment based on the Langevin framework was used in [23] for predicting fission-fragment mass distribution. Langevin equations for the five-dimensional shape parameter were solved to calculate the fission-fragment mass distribution. The mass and charge yields for the fission of ^{234}U at $E^* = 11$ MeV were studied at different damping energy values. Benchmarking of the 70 fission-fragment charge yields was done against the measured yields. Langevin equations in a five-dimensional space of nuclear deformations were solved in [24] to study the fission of nuclei at low and medium excitation energies. They measured the fragment mass yield and kinetic energy by varying the incident energy of the neutron.

The fission fragment mass yields for 987 nuclides have been evaluated using the benchmarked Brownian shape-motion method [25]. In Ref. [26], a four-dimensional Langevin dynamical model was developed employing $\{c, h, \alpha\}$ parametrization to generate nuclear shape. The evolution of the collective coordinates was treated as the motion of Brownian particles and then coupled Langevin equations were solved. The parameters of the mass-energy distribution of fission fragments, fission time, fission rate, the angular distribution of fission fragments, and prescission particle multiplicities were also studied.

In Ref. [27], Gherghescu *et al.* studied the dynamics of the fission process and the associated nuclear shapes for deformed fragments within the framework of the two-center shell model. It is shown that cold energy valleys due to the deformed shell structure of the fragments can be studied in this deformed two-center shell model for the fissioning of a deformed parent nucleus into deformed fragments. The level schemes and the shell correction energy were evaluated for the fission of $^{306}122$ and ^{252}Cf. The deformed two-center shell model developed for ellipsoidal fission fragments was applied for the experimentally studied fusion reactions and for the synthesis of the superheavy nucleus $^{296}116$ [28]. Poenaru *et al.* studied the nuclear shapes for binary, ternary, and quaternary fission by solving integrodifferential equations based on the liquid-drop model [29].

We used the dynamical cluster decay model (DCM) developed by Gupta and collaborators in this work to study the neutron-induced reactions, with the following two aspects, which thus far have not been studied within DCM.

(1) The temperature considered so far is a constant value for all decaying channels corresponding to the excitation energy of the compound nuclear (CN) system. However, if a constant temperature is used to evaluate the excitation energies of the fragments of each channel, then the sum of the excitation energies of the fissioning fragments is found to be not equal to the excitation energy of the compound nucleus. This requirement demands different temperatures for different channels, so that their total excitation energy is conserved. Such temperature tuning has been demonstrated by one of us recently in the studies of ternary fission [30], which has been now extended in DCM to the neutron-induced fission of ^{235}U.

(2) The DCM stems from the ideas of quantum mechanical fragmentation theory, which considers the dynamical collective mass motion of the preformed fragments (channels) through the confining potential barrier. The success of the DCM is the treatment of light-particle emission and intermediate-mass fragment emission, as well as fission-fragment emission in the same footing, unlike other models, such as the scission-point or saddle-point models, which treat particle emission and fission-fragment emission separately. One of the important concepts considered in DCM is the probability of preformation of fragments. For fissile systems like U, experimentally, the mass distributions are reported to be confined to a particular mass window. In this work, the role of mass window restriction and the preformation probability are analyzed within DCM.

The role of neck distance and excitation energy is also studied, in addition to the temperature tuning, mass window restriction. The model description is discussed in the following section. In the subsequent sections, the calculation and results are presented, followed by a summary.

II. METHOD

The dynamical cluster-decay model is a nonstatistical description developed by Gupta and collaborators [31–33] based on the preformed cluster model (PCM) of Gupta *et al.* [34–37] which in turn is based on quantum mechanical fragmentation theory (QMFT) [37–39] developed for the ground-state decays. QMFT, a unified description of both fission and fusion
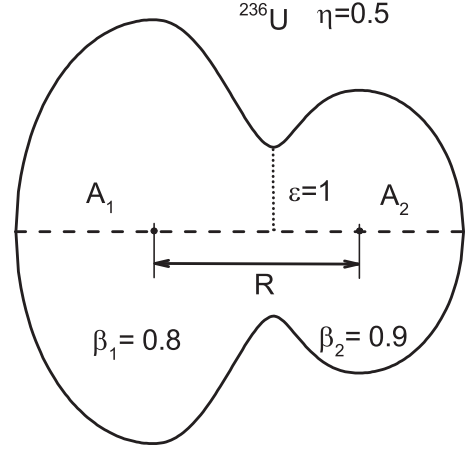
FIG. 1. Explanation of the coordinates used in QMFT. Shown is the shape of the nuclear system obtained in the fissioning of ^{236}U with $\eta = 0.5$, $\beta_1 = 0.8$, $\beta_2 = 0.9$, and $\varepsilon = 1$.

of nuclei, gives a dynamical evolution of fissioning systems. This theory is based on the two-center shell model and is worked in terms of the measurable coordinates of mass and charge fragmentations and a few collective coordinates given as follows: (i) the relative separation coordinate R between the two nuclei or fragments, (ii) intrinsic structure of two nuclei defined in terms of β_1 and β_2, (iii) neck parameter ε, and (iv) mass- and charge-fragmentation coordinates η and η_Z. The coordinates used in QMFT are represented in Fig. 1. The two dynamical collective coordinates [39] of mass η and charge asymmetry η_Z of two fragments are defined as

$$\eta = \frac{(A_1 - A_2)}{(A_1 + A_2)}; \quad \eta_Z = \frac{(Z_1 - Z_2)}{(Z_1 + Z_2)}. \quad (1)$$

The subscripts 1 and 2 refer respectively to the heavy and light fragments. $|\eta| = 1$ corresponds to the complete fusion of nuclei and $\eta = 0$ indicates symmetric fission of nuclei. The collective Hamiltonian in terms of collective coordinates and their velocities is given as

$$H = T(R, \beta, \eta, \eta_Z; \dot{R}, \dot{\beta}, \dot{\eta}, \dot{\eta_Z}) + V(R, \beta, \eta, \eta_Z), \quad (2)$$

where the kinetic energy in terms of mass parameters B_{ij} is

$$\begin{aligned} T = {}& \tfrac{1}{2} B_{RR} \dot{R}^2 + \tfrac{1}{2} B_{\beta\beta} \dot{\beta}^2 + \tfrac{1}{2} B_{\eta\eta} \dot{\eta}^2 + \tfrac{1}{2} B_{\eta_Z\eta_Z} \dot{\eta_Z}^2 \\ & + B_{R\beta} \dot{R}\dot{\beta} + B_{R\eta} \dot{R}\dot{\eta} + B_{R\eta_Z} \dot{R}\dot{\eta_Z} \\ & + B_{\beta\eta} \dot{\beta}\dot{\eta} + B_{\beta\eta_Z} \dot{\beta}\dot{\eta_Z} + B_{\eta\eta_Z} \dot{\eta}\dot{\eta_Z}. \end{aligned} \quad (3)$$

The collective potential V is evaluated based on the Strutinsky macro-microscopic approach with the macroscopic part contributed by the liquid-drop model (LDM) and the microscopic part by the single-particle energies of the asymmetric two-center shell model (ATCSM). The single-particle levels are used to obtain the shell corrections. A detailed account of the shell effect in TCSM has been presented in Ref. [27]. The resulting Hamiltonian after minimizing the collective potential in ε, β_1, and β_2 for the η motion is

$$H(\eta, R) = \tfrac{1}{2} B_{RR} \dot{R}^2 + \tfrac{1}{2} B_{\eta\eta} \dot{\eta}^2 + B_{R\eta} \dot{R}\dot{\eta} + V(R, \eta). \quad (4)$$

The coupling mass $B_{R\eta}$ can be neglected. Using these, the time-dependent Schrödinger equation for coupled η (including mass and charge asymmetry) and R coordinates can be constructed as

$$H(\eta, R)\Psi(\eta, R, t) = i\hbar \frac{\partial}{\partial t}\Psi(\eta, R, t), \qquad (5)$$

with the Hamiltonian constructed as

$$H(\eta, R) = -\frac{\hbar^2}{2\sqrt{B_{\eta\eta}}}\frac{\partial}{\partial \eta}\frac{1}{\sqrt{B_{\eta\eta}}}\frac{\partial}{\partial \eta} - \frac{\hbar^2}{2\sqrt{B_{RR}}}\frac{\partial}{\partial R}\frac{1}{\sqrt{B_{RR}}}\frac{\partial}{\partial R}$$
$$+ V(\eta) + V(R) + V(\eta, R). \qquad (6)$$

The coupling term in the potential $V(\eta, R)$ is small and so after the separation of variables, we obtain

$$\Psi(\eta, R, t) = \psi(\eta, t)\phi(R, t). \qquad (7)$$

For the η motion (at fixed R),

$$\left[-\frac{\hbar^2}{2\sqrt{B_{\eta\eta}}}\frac{\partial}{\partial \eta}\frac{1}{\sqrt{B_{\eta\eta}}}\frac{\partial}{\partial \eta} + V(\eta)\right]\psi(\eta, t) = i\hbar\frac{\partial}{\partial t}\psi(\eta, t). \qquad (8)$$

For the R motion (at fixed η),

$$\left[-\frac{\hbar^2}{2\sqrt{B_{RR}}}\frac{\partial}{\partial R}\frac{1}{\sqrt{B_{RR}}}\frac{\partial}{\partial R} + V(R)\right]\phi(R, t) = i\hbar\frac{\partial}{\partial t}\phi(R, t). \qquad (9)$$

Assuming the fission to be an adiabatic process, η and η_Z motions can be considered as fast compared to the relative R motion. R motion is slow after the system has tunneled through the barrier and so R can be taken as a time-independent parameter. Therefore, we consider the η motion at fixed R and the corresponding Schrödinger equation. The dynamics in fission process or the fission charge (and mass) distributions remain the same from saddle (R_{saddle} or $R_{\text{saddle}} + \Delta R$) to scission point. The η_Z motion can be solved analytically for fixed R ($= R_{\text{saddle}} + \Delta R$) value under the initial condition of a narrow Gaussian distribution. The calculations show that the charge (and mass) distributions get fixed at an R value very close to the saddle point and remain fixed till the scission configuration by running down the Coulomb barrier. The role of coupling of η motion to the relative R motion is studied using the Hill and Wheeler penetrability [40] and through a parametrized friction [41]. Comparing both the results with the experimental data indicate that the coupling effects of η and $R(t)$ motions are weak. Hence, in this work as in other DCM calculations, we will consider the η motion alone at fixed R (more specifically at the saddle point). The stationary Schrödinger equation in the η coordinate at a fixed R value can be written more precisely as

$$\left[-\frac{\hbar^2}{2\sqrt{B_{\eta\eta}}}\frac{\partial}{\partial \eta}\frac{1}{\sqrt{B_{\eta\eta}}}\frac{\partial}{\partial \eta} + V(\eta)_R\right]\psi_R^{(\nu)}(\eta) = E_R^{(\nu)}\psi_R^{(\nu)}(\eta). \qquad (10)$$

Here, η_Z is fixed for η motion by the charge minimization procedure. The kinetic energy part is represented using the classical hydrodynamical mass of Kröger and Scheid [42] which is shown to compare with the microscopic cranking
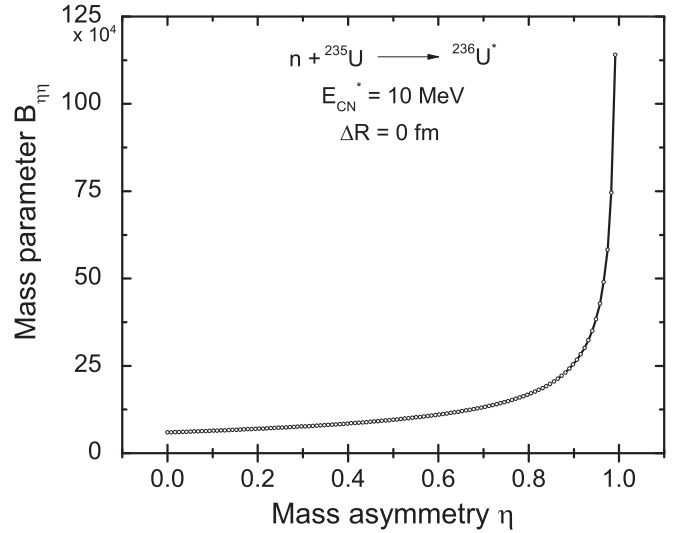
FIG. 2. Smooth hydrodynamical mass parameters $B_{\eta\eta}$ as a function of mass asymmetry.

masses. In Fig. 2, the smooth hydrodynamic mass is presented as a function of mass asymmetry. Any explicit temperature dependence is not considered in evaluating $B_{\eta\eta}$ values and hence the constant mass means a complete washing of shell effects in it. Further, for the actual calculations, the shell corrections are not calculated explicitly from the two-center shell model, rather, the analytical expression of Myers and Swiatecki is used. As the static potentials $V(\eta)_R$ contain important information concerning fission, fusion, and cluster radioactivity, we consider that the potential at the touching configuration would carry the necessary information. In the asymptotic region, the collective potential is the sum of experimental binding energies of two fragments, the Coulomb and nuclear interaction between them, given by

$$V(\eta)_R = -\sum_{i=1}^{2} B(A_i, Z_i) + \frac{Z_1 Z_2 e^2}{R} + V_N, \qquad (11)$$

$\psi_R^\nu(\eta)$ are the vibrational states in the potential $V(\eta)$, and ν has values as $\nu = 0, 1, 2, \ldots$ with $\nu = 0$ referring to the ground state. Here $\psi_R^{(\nu)}$ is the eigenwavefunction obtained with the energy eigenvalue as $E_R^{(\nu)}$. For spontaneous fission, only the lowest vibrational state ($\nu = 0$) should be occupied. The mass (or charge) distribution yield of finding a certain mass (or charge) fragmentation at a position R on the fission path and normalized to 200% is given in general as

$$Y(f_i) = |\psi_R(\eta(f_i))|^2 \sqrt{B_{\eta\eta}(f_i)}\frac{200\%}{A_{\text{CN}}/2}, \qquad (12)$$

with $f_i = A_i$ or $Z_i, i = 1$ or 2. Normalizing and scaling $|\psi(\eta)|^2$ to give the fractional mass yield, at mass A_2 of the cluster, is defined as preformation probability P_0 for the ground-state decay, and normalization to 2 is given by

$$P_0(A_2) = |\psi(\eta)|^2 \sqrt{B_{\eta\eta}}\left(\frac{2}{A_{\text{CN}}}\right). \qquad (13)$$
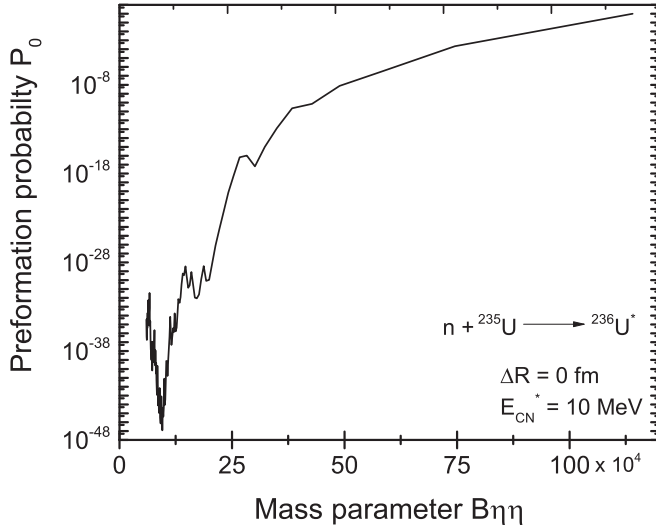
FIG. 3. Preformation probability P_0 as a function of hydrodynamical mass parameter $B_{\eta\eta}$.

If the nucleus fissions from an excited state or if the coupling between R and η degrees of freedom causes some internal excitation, then higher states in η become excited and so temperature effects have to be included. The excitations of higher vibrational states are included through a Boltzmann-like occupation of excited states. Thus, we define the preformation probability P_0 as

$$|\psi_R|^2 = \sum_{\nu=0}^{\infty} |\psi_R^{(\nu)}|^2 \exp\left(-E_R^{(\nu)}/T_{CN}\right). \quad (14)$$

T_{CN} is the nuclear temperature or the temperature of the compound nucleus (in MeV) of mass A_{CN} and is related to the excitation energy E_{CN}^* through a semiempirical statistical relation [43,44]

$$E_{CN}^* = \frac{A_{CN}}{9} T_{CN}^2 - T_{CN}. \quad (15)$$

Here, for the compound nucleus $^{236}U^*$, the excitation energy E_{CN}^* of 10 MeV corresponds to a temperature of 0.636 MeV, and this is the temperature of the compound nucleus formed. In Fig. 3, we present the calculated preformation probability as a function of the mass parameter for the compound nucleus $^{236}U^*$ corresponding to an excitation energy of 10 MeV. The structural information contained in the preformation probability is actually due to the static potential defined in Eq. (11), rather than the mass parameters. The mass parameter values are considered for all the mass asymmetry in this figure. In DCM, the complex fragments [the intermediate mass fragments (IMFs) or clusters] are treated as a dynamical collective mass motion of preformed fragments through the barrier. At fixed R, the fission process depends on the temperature as well as on η. The energy transfer in the incident path is

$$E_{c.m.} + Q_{in} = E_{CN}^* = (E_1^* + E_2^*)_{saddle}. \quad (16)$$

The sum of kinetic energy $E_{c.m.}$ and Q value of the entrance channel gives the excitation energy of the compound nucleus E_{CN}^*. Here E_1^* and E_2^* are the excitation energies of the two

fragments at the saddle. Thus far in DCM, the temperature is assumed to be the same for all outgoing fission channels in the binary breakup of the compound nucleus. However, the sum of excitation energy of the two fragments evaluated with this temperature gives a value larger than E_{CN}^*. Hence, we attempt here to include specific temperature for each channel. The excitation energy of the equilibrated compound system E_{CN}^* in the thermal equilibrium at a fixed distance R (say at a saddle distance) is shared as the individual excitation energies of the two fragments. The fission energy will be due to the running down of the fragments under Coulomb repulsion.

As noted earlier, the concept of using fixed T_{CN} for all outgoing channels does not conserve energy as in Eq. (16). Hence, the temperature for each channel is iteratively tuned such that the sum of their excitation energies is always approximately equal to E_{CN}^* [30]. To calculate the temperature for each channel, an arbitrary initial temperature is considered. Then the temperature-dependent binding energy [45] [given in Eq. (19)] of two fragments in a particular channel is calculated corresponding to this arbitrary temperature and their respective excitation energies are evaluated as the difference in binding energies at the specific temperature to that at ground state as

$$E_i^*(A_i, Z_i) = B.E(T, A_i, Z_i) - B.E(T=0, A_i, Z_i,), \quad (17)$$

with $i = 1, 2$ for the two fragments. The arbitrary temperature is tuned such that the sum total of individual excitation energies of the fragments is equal to the excitation energy of the compound nucleus, i.e., $E_1^*(A_1, Z_1) + E_2^*(A_2, Z_2) \approx E_{CN}^*$. The temperature thus obtained is referred to as the channel temperature T_η. The variation of this channel temperature is presented in Fig. 4(a) corresponding to the compound nucleus excitation energy of $E_{CN}^* = 10$ MeV. The dashed line in this figure is the temperature of the compound nucleus ($T_{CN} = 0.636$ MeV). Figure 4(b) presents the excitation energies of the fragments corresponding to the channel temperatures presented in Fig. 4(a). The sum of these excitation energies would give the total energy of 10 MeV ($\approx E_{CN}^*$). This channel temperature is further used in the calculation of fragmentation potential energy $V_R(\eta, T_\eta)$ [Eq. (11)] along with the damping of shell effect which decays exponentially. The potential is

$$V_R(\eta, T_\eta, l) = \sum_{i=1}^{2}[BE_{LDM}(A_i, Z_i, T_\eta)]$$
$$+ \sum_{i=1}^{2}(\delta U_i) \exp\left(-\frac{T_\eta^2}{T_0^2}\right) + V_C(T_\eta) + V_P(T_\eta). \quad (18)$$

$BE_{LDM}(T_\eta)$ is the temperature-dependent binding energy calculated from the expression given by Krappe in [45]. This binding energy expression contains temperature-dependent Wigner and pairing terms in addition to the temperature-dependent liquid-drop term. The temperature-dependent mass formula is given by

$$E(Z, N, shape, T) = M_H Z + M_n N + E_{ld}(T) + E_W + E_{pair}$$
$$+ f(k_f r_p)\frac{Z^2}{A} - c_a(N-Z) - a_{el}Z^{2.39}, \quad (19)$$
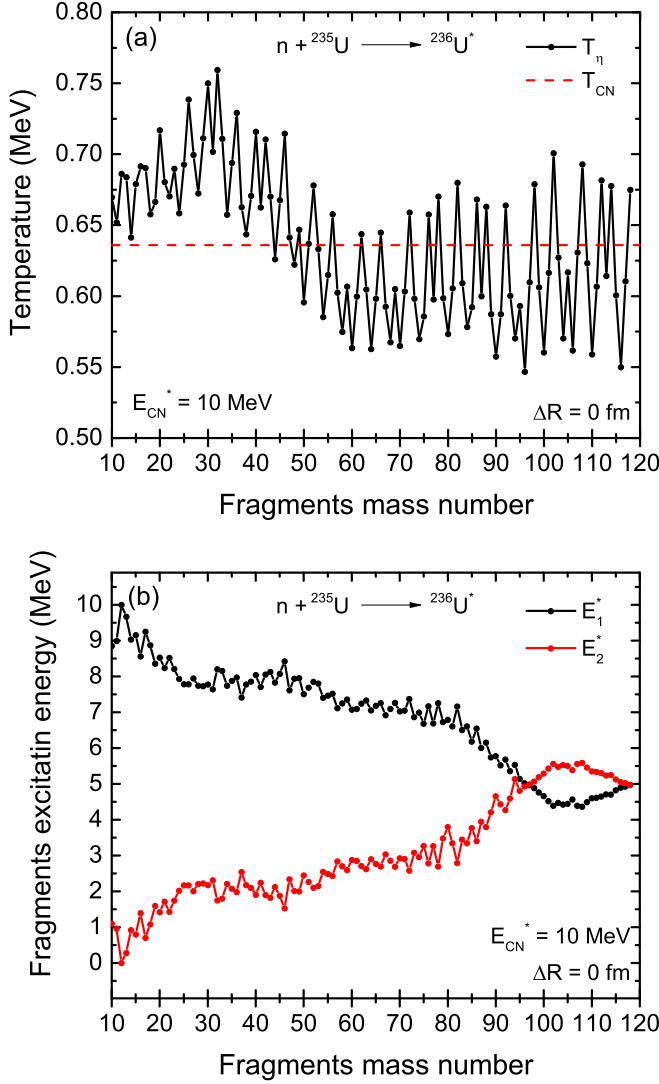
FIG. 4. (a) Variation of channel temperature obtained by conserving the excitation energies plotted as a function of the fragment mass number for $E_{CN}^* = 10$ MeV and $\Delta R = 0$ fm. (b) Excitation energies of fragments A_1 and A_2, whose sum would be equal to the compound nucleus excitation energy $E_{CN}^* = 10$ MeV, plotted as a function of fragment mass number.

with $M_H = 7.289$ MeV, $M_n = 8.071$ MeV, Fermi wave number $k_f = \left(\frac{9\pi Z}{4A}\right)^{1/3} r_0^{-1}$, $c_a = 0.145$ MeV, $r_p = 0.80$ fm, and $a_{el} = 1.433 \times 10^{-5}$. The proper liquid-drop energy is given as

$$E_{ld} = -a_V(1 - k_V I^2)A + a_S(1 - k_S I^2)B_1 A^{2/3} + c_0 A^0$$
$$+ c_1 \frac{Z^2}{A^{1/3}} B_3 - c_4 \frac{Z^{4/3}}{A^{1/3}}, \quad (20)$$

where $I = (N - Z)/(N + Z)$ is the neutron excess parameter and the seven parameters $r_0, a, a_{den}, a_V, k_V, a_S$, and k_S are assumed to have quadratic temperature dependence and are defined as $a_j(T_\eta) = a_j(T = 0)(1 - x_j T_\eta^2)$. Their values are taken as in [45].

The second terms in Eq. (18) correspond to the shell corrections, calculated from the analytical expression by Myers and Swiatecki [46] and are considered to vanish exponentially with temperature. $V_C(T_\eta)$ and $V_P(T_\eta)$ in Eq. (18) are respectively the T-dependent Coulomb potential and the nuclear proximity potential based on [47]. The temperature dependence in Coulomb and proximity potential are included through the radius expression given by

$$R_i(T_\eta) = 1.16\left(1 + 7.63 \times 10^{-4} T_\eta^2\right) A_i^{1/3} \text{ fm.} \quad (21)$$

Here $i = 1$ and 2 correspond respectively to the heavy and light fragments. The temperature-dependent Coulomb energy is

$$V_C(T_\eta) = \frac{Z_1 Z_2 e^2}{R(T_\eta)} \text{ MeV}, \quad (22)$$

with $R(T_\eta)$ as the relative separation distance between the centers of the fragments, and $R(T)$ at the touching point is denoted as $R(T_\eta) = R_t(T_\eta) = R_1(T_\eta) + R_2(T_\eta) + \Delta R(T_\eta)$. The center to center distance can be varied by the term $\Delta R(T_\eta)$, known as the neck distance which takes the value of zero when the surfaces of the two fragments are touching. Any higher value of ΔR refers to the separated fragments by the distance of ΔR. The neck parameter ε defined earlier to represent the two-center shape is connected to ΔR corresponding to the no-neck configuration, since we consider the fragments to be spherical ($\beta_i = 0$) and the calculations at fixed ΔR from the touching configuration and beyond. The nuclear proximity potential is defined as

$$V_P(T_\eta) = 4\pi \bar{R}(T_\eta)\gamma b(T_\eta)\phi[s(T_\eta)] \text{ MeV}, \quad (23)$$

with $\bar{R}(T)$ defining the inverse of the rms radius of the Gaussian curvature. $\phi[s(T_\eta)]$ and γ are universal functions independent of the geometry of the system and the nuclear surface energy coefficient, respectively. The proximity potential of Blocki *et al.* [47] is a surface effect which plays an important role in the physics of heavy-ion collisions. The interacting force between two gently curved surfaces in proximity is given in terms of a geometrical factor representing the mean curvature of the interacting surface and a universal function of separation. The universal function gives the interaction potential per unit area between two flat surfaces. In Ref. [48] the semiclassical extended Thomas Fermi (ETF) approach based on Skyrme forces was used to evaluate the universal function. Various terms used in Eq. (23) are

$$\gamma = 0.9517\left[1 - 1.7826\left(\frac{N - Z}{A}\right)^2\right] \text{MeV fm}^{-2}, \quad (24)$$

$$\phi[s(T_\eta)]$$
$$= \begin{cases} -\frac{1}{2}(s - 2.54)^2 - 0.0852(s - 2.54)^3, & s \leqslant 1.2511, \\ -3.437\exp(-s/0.75), & s \geqslant 1.2511. \end{cases}$$
$$(25)$$

$$s(T_\eta) = \frac{R(T_\eta) - [R_1(T_\eta) + R_2(T_\eta)]}{b(T_\eta)} \quad (26)$$

is the separation distance between the two surfaces with

$$b(T_\eta) = 0.68\left(1 + 7.37 \times 10^{-3} T_\eta^2\right) \text{ fm}. \quad (27)$$

The pairing and shell correction terms, though essential for reproducing the ground-state binding energies, do not have much significance at higher excitation energies as is shown in [49]. The contributions of pairing and shell corrections vanish beyond the temperature value of 2 MeV. However, the Wigner term has a significant contribution in the mass formula and does not vanish up to the temperature of around 4 MeV.

In the present work, we consider only the η motion, since it would give the required mass distribution. The R motion and the cross-section calculations as done in DCM are not attempted here.

III. RESULTS AND DISCUSSION

In the fission mass distribution studies, the most probable mass and charge numbers of fission fragments can be chosen either by taking charge to mass ratio of the fissioning fragments to be equal to the charge to mass ratio of the fissioning nucleus as

$$\frac{Z_{\text{CN}}}{A_{\text{CN}}} = \frac{Z_i}{A_i}, \quad (28)$$

or by minimizing the potential energy. Plenty of other methods also exist to estimate the fragmentation yields such as the methods developed in [50,51], where the particle number formalism is used to extract the fragmentation associated with the quasiparticle Slater determinants. However, for the sake of simplicity, we estimate the fragmentation by using one of the above two methods, namely, the charge to mass ratio method. In Eq. (28), Z_{CN}, A_{CN} and Z_i, A_i ($i = 1, 2$) stand respectively for charge and mass number of compound nuclei and for the two fragments. This empirical equivalence of charge to mass ratio is found to agree with experimental mass distribution. Once, using this conservation, the entire mass asymmetry is obtained; then the corresponding fragmentation potential at given excitation energy and in turn the probability can be computed as discussed above.

In the method of minimizing potential energy, the fragmentation potential as defined in Eq. (18) can be calculated for a given mass asymmetry for all possible charge asymmetries. The probability is computed by minimizing the potential energy corresponding to a particular charge asymmetry. Though the former method is empirical, the computation is easy, as one is limited only to one charge asymmetry for a given mass asymmetry. Due to the tuning of temperature in the present study, this method is more convenient. However, the second method is cumbersome, since all the charge asymmetries are to be considered for a given mass asymmetry and further, with temperature tuning, the charge minimization of the fragmentation potential becomes computationally intensive.

For the present work, both these methods are considered. The first method is initially considered to understand the role of mass window restriction, excitation energy, and neck length. From the results obtained, for a chosen mass window, excitation energy, and neck length, the calculations are done using the second method, by properly charge minimizing the
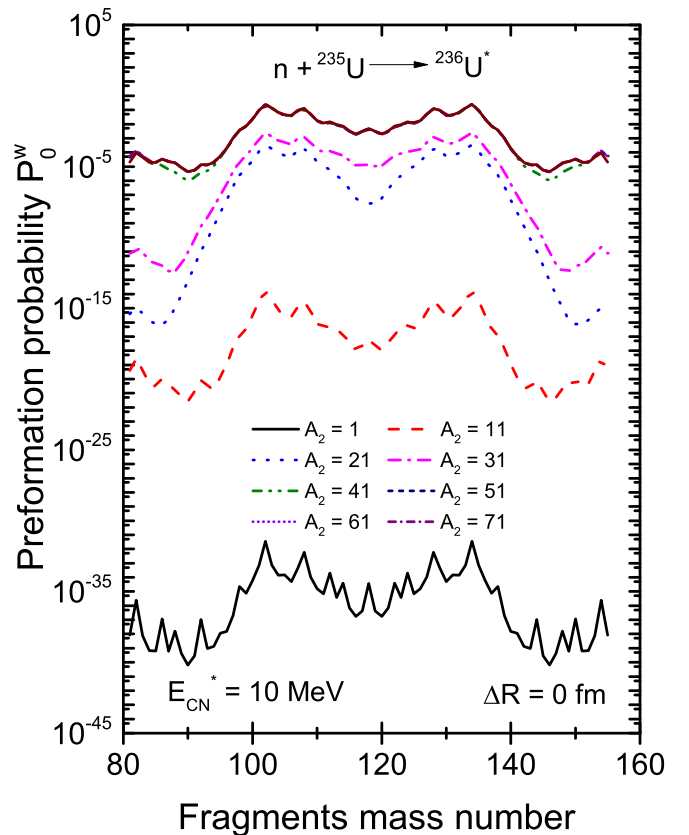
FIG. 5. Mass window variation in the yield and/or mass distributions as a function of the mass number of the fragments for different windows at compound nucleus excitation energy 10 MeV and $\Delta R = 0$ fm. For each mass window, the calculations are done starting from the mentioned A_2 values up to $A_2 = 118$ and its reflected values, but shown only for the mass range of 80–156.

fragmentation potential energy with the tuning of temperature. Experimentally, the reported fission mass distribution is limited to a restricted mass range and accordingly in this work, we report the role of the mass window in the probability calculation of fission mass distribution. However, in fragmentation theory, the probability for the entire mass asymmetry can be studied.

Figure 5 presents the calculated preformation probability as a function of the mass number of fission fragments for various mass windows, corresponding to the excitation energy of 10 MeV and a neck distance of 0 fm. It is to be mentioned here that the potential energy is minimized at a static distance and smooth hydrodynamical masses are used instead of minimizing the action integral for proper dynamical treatment. However, though explicit effects of temperature and shell effects are not considered in evaluating the mass parameter $B_{\eta\eta}$, the obtained results exhibit a structural variation in the preformation probability indicating that the use of constant mass inertia tensor and fixed distance between the centers also accounts for the observed structural variation. In this figure, various lines correspond to the calculation of different mass windows but only plotted for the mass range of 80–160. The solid line corresponds to all possible binary fragmentation starting from
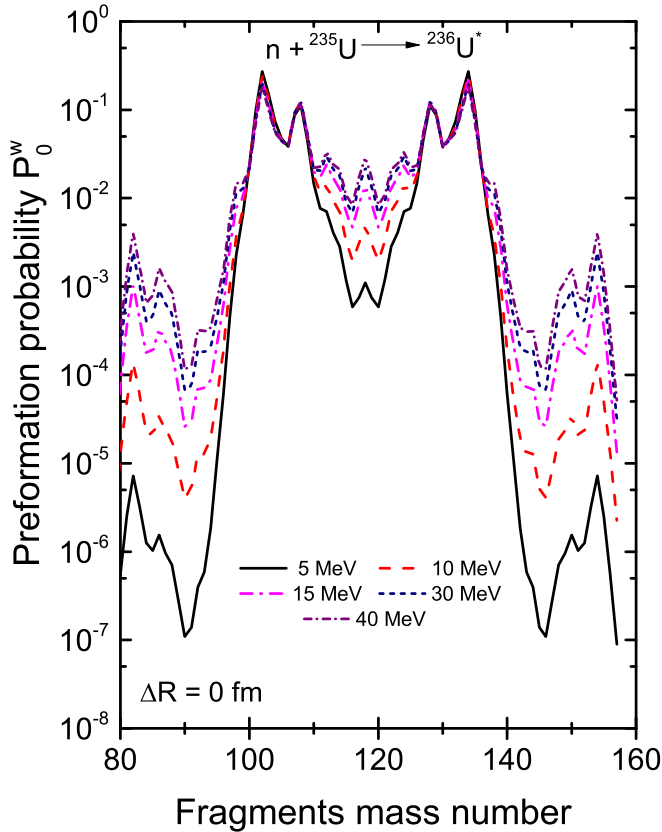
FIG. 6. Excitation energy variation in the yield distribution for a fixed mass window from $A_2 = 80$ to 156 and $\Delta R = 0$ fm.

FIG. 7. Neck length variation in the yield distribution for a fixed mass window from $A_2 = 80$ to 156 and $E_{CN}^* = 10$ MeV.

$A_2 = 1$ with mass asymmetry nearly equal to 0.99 to $A_2 = 118$ with mass asymmetry equal to zero. The probability values are reflected beyond 118, and the total probability is normalized to 2. For this case, the magnitude of the probability for the fragments in the near-symmetric region is found to be very low (10^{-30} to 10^{-35}). This is because, for very light particles, the probability is found to be very large. If the mass window is restricted, say, by not considering fragments up to $A_2 = 10$, and considering only from $A_2 = 11$ to $A_2 = 118$, a drastic change in the magnitude of the probability is seen. Nearly 20 orders of magnitude difference is seen in the probability values. For this case, the magnitude for the fragments in the near-symmetric region is found to be around 10^{-15}. However, in both these cases, the fragments corresponding to the maximum yield remains the same, except for its magnitude. A further restriction of mass window is shown for $A_2 = 21$ to 118, $A_2 = 31$ to 118, $A_2 = 41$ to 118, $A_2 = 51$ to 118, $A_2 = 61$ to 118 and $A_2 = 71$ to 118. For the $A_2 = 21$ and $A_2 = 31$ windows, a larger variation for lighter fragments is seen, but the probability values become comparable for fragments in the near-symmetric region. Moreover, the strong minima seen corresponding to symmetric breakup for the $A_2 = 21$ mass window become shallower for the $A_2 = 31$ mass window. With the further restriction in the mass window, corresponding to $A_2 = 41$ to $A_2 = 81$, the probability values are found to converge. Thus, the restriction of the mass window significantly alters the magnitude of the

probability values. However, the most probable fragment pair in all windows remains the same except for its magnitude. For further calculations, we consider a restricted mass window of $A_2 = 79$ to $A_2 = 118$, similar to the experimental mass window.

The role of excitation energy with temperature tuning is studied and presented in Fig. 6. The preformation probability values denoted as P_0^w, with w referring to mass window restriction, corresponding to a neck distance of $\Delta R = 0$ fm is plotted against fragment mass number for different excitation energies from $E_{CN}^* = 5$–40 MeV. As is known, the increase in excitation energy increases the probability values; more or less a linear scaling in the increase is seen except around the symmetric region. The deeper minimum seen corresponding to the symmetric fragments is found to become shallower as the excitation energy increases. Irrespective of different excitation energies considered, the most probable fragment pair remains the same.

The role of neck distance is presented in Fig. 7. For the restricted mass window and fixed excitation energy of $E_{CN}^* = 10$ MeV, different neck distances are considered from 0 to 3 fm. For $\Delta R = 0$ and 1 fm, linear scaling with a decrease in probability values is seen. However, structural variations are present in the preformation probability values in the asymmetric region around mass numbers 80–90 with an increase in the neck distance. There is no significant change in the preformation probability values around the near-symmetric and symmetric regions for various neck distances considered.
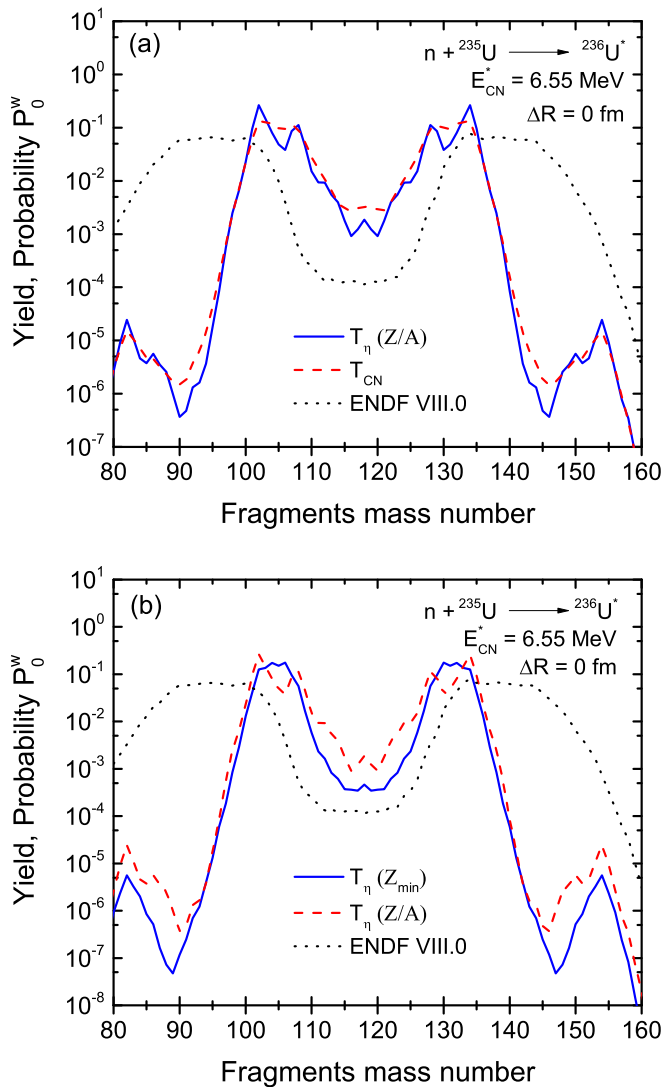
FIG. 8. (a) Comparison of our calculated mass distribution using fixed excitation energy denoted as T_η (Z/A) and fixed temperature denoted as T_{CN} with the experimental values taken from Ref. [52] plotted as a function of the mass number of the fragments. The excitation energy E^*_{CN} is 6.5 MeV, $\Delta R = 0$ fm for a mass window restriction of $A_2 = 79$ to 157. (b) Same as (a), but for fixed excitation energy computed using the Z/A method denoted as T_η (Z/A) and a charge minimization method denoted as $T_\eta(Z_{min})$.

The neck distance of $\Delta R = 0$ fm is found to have a maximum preformation probability. Hence we use $\Delta R = 0$ fm for the study.

The experimental yield values corresponding to thermal neutron-induced reactions are taken from ENDF/B-VIII.0 [52] for the comparison of our results of mass distribution. Corresponding to the experimental energy, excitation energy of $E^*_{CN} = 6.5$ MeV is considered in the calculations at a neck distance of 0 fm. The calculated values using the charge to mass ratio conservation method with tuned temperature as well as the fixed temperature corresponding to the excitation energy are presented in Fig. 8(a). The double-humped distribution is seen in both calculations. The tuning of temperature

results in some structural details, whereas the distribution is smooth when a constant temperature is considered for all the channels. Compared to experimental distribution, the calculated double-humped structure (solid and dashed lines) is narrower with the largest value for fragments with mass numbers $A_2 = 102$ and $A_1 = 134$ and $A_2 = 108$ and $A_1 = 128$. It is to be mentioned that, the experimental yield values are for the separated fragments which underwent a transition from a mononucleus to two fragments along the deformation coordinate. However, the calculations are limited to the mass asymmetry motion, and the relative motion is not considered. Hence, the comparison is only a qualitative comparison as has been reported earlier in the statistical scission-point models [15,16,53].

Figure 8(b) presents similar results corresponding to the charge to mass ratio conservation method and potential energy minimization method for obtaining the tuned channel temperatures. Both the calculations, more or less, have a similar structure with the latter exhibiting a smooth variation. Our calculated yield at peak values is associated with a closed shell of the fragments. The peak corresponding to $A_2 = 102$ and $A_1 = 134$ may be attributed to the nearly closed shell of the proton number ~ 52 of the fragment $A_1 = 134$ mass. The other peak for the mass numbers $A_2 = 82$ and $A_1 = 154$ may be attributed to the closed-shell neutron number ~ 50 associated with A_2.

IV. SUMMARY

The dynamical cluster decay model has been used to study the neutron-induced fission reaction forming $^{236}U^*$ by considering two different aspects: temperature tuning for each mass asymmetry value and restriction of the mass window. The idea of a channel temperature is studied for the first time instead of a fixed temperature as used in DCM in earlier studies. The proper conservation of excitation energy between the fragments with respect to the excitation energy of the parent nucleus is ensured. The role of mass window restriction is demonstrated to have a significant effect on the magnitude of the probability values of the mass distributions. It is shown that as the mass window is narrowed down, the probability values are found to converge. The variation of excitation energy results in a linear scaling of the mass distribution with an increase in excitation energy. The effect of neck length is also studied. The computed probabilities using fixed excitation energy and hence in turn, various channel temperatures, as well as fixed temperature, are compared with available experimental yield values, and a qualitative comparison is seen. Studying the role of relative motion within this model is planned. The applicability of this idea of temperature tuning will be studied in low-energy light-mass and medium-mass compound systems formed in heavy-ion induced reactions.

ACKNOWLEDGMENTS

[1] M. R. Pahlavani and S. M. Mirfathi, Phys. Rev. C **92**, 024622 (2015).

[2] B. Becker, P. Talou, T. Kawano, Y. Danon, and I. Stetcu, Phys. Rev. C **87**, 014617 (2013).

[3] H. Pasca, A. V. Andreev, G. G. Adamian, N. V. Antonenko, and Y. Kim, Phys. Rev. C **93**, 054602 (2016).

[4] C. Romano, Y. Danon, R. Block, J. Thompson, E. Blain, and E. Bond, Phys. Rev. C **81**, 014607 (2010).

[5] C. Paradela, M. Calviani, D. Tarrío, E. Leal-Cidoncha *et al.* (n_TOF Collaboration), Phys. Rev. C **91**, 024602 (2015).

[6] https://www-nds.iaea.org/standards/Data/endf-6-format/std-092_U_235.endf ().

[7] https://www-nds.iaea.org/standards/Data/endf-6-format/std-092_U_238.endf ().

[8] R. Yanez, L. Yao, J. King, W. Loveland, F. Tovesson, and N. Fotiades, Phys. Rev. C **89**, 051604(R) (2014).

[9] K. H. Schmidt, B. Jurado, and C. Amouroux, http://www.khs-erzhausen.de/GEF.html.

[10] R. Yanez, J. King, J. Barrett, W. Loveland, N. Fotiades, and H. Lee, Nucl. Phys. A **970**, 65 (2018).

[11] K.-H. Schmidt, B. Jurado, C. Amouroux, and C. Schmitt, Nucl. Data Sheets **131**, 107 (2016), special Issue on Nuclear Reaction Data.

[12] M. Lebois, J. N. Wilson, P. Halipré, A. Oberstedt, S. Oberstedt, P. Marini, C. Schmitt, S. J. Rose, S. Siem, M. Fallot, A. Porta, and A.-A. Zakari, Phys. Rev. C **92**, 034618 (2015).

[13] A. Chyzh, C. Y. Wu, E. Kwan, R. A. Henderson, T. A. Bredeweg, R. C. Haight, A. C. Hayes-Sterbenz, H. Y. Lee, J. M. O'Donnell, and J. L. Ullmann, Phys. Rev. C **90**, 014602 (2014).

[14] A. Oberstedt, T. Belgya, R. Billnert, R. Borcea, T. Bryś, W. Geerts, A. Göök, F.-J. Hambsch, Z. Kis, T. Martinez, S. Oberstedt, L. Szentmiklosi, K. Takàcs, and M. Vidali, Phys. Rev. C **87**, 051602(R) (2013).

[15] J.-F. Lemaître, S. Panebianco, J.-L. Sida, S. Hilaire, and S. Heinrich, Phys. Rev. C **92**, 034617 (2015).

[16] B. Wilkins and E. Steinberg, Phys. Lett. B **42**, 141 (1972).

[17] C. Karthika and M. Balasubramaniam, Eur. Phys. J. A **55**, 59 (2019).

[18] N. Schunck, D. Duke, and H. Carr, Phys. Rev. C **91**, 034327 (2015).

[19] A. Bulgac, P. Magierski, K. J. Roche, and I. Stetcu, Phys. Rev. Lett. **116**, 122504 (2016).

[20] H. Goutte, J. F. Berger, P. Casoli, and D. Gogny, Phys. Rev. C **71**, 024316 (2005).

[21] D. Regnier, N. Dubray, and N. Schunck, Phys. Rev. C **99**, 024611 (2019).

[22] K. Pomorski, B. Nerlo-Pomorska, J. Bartel, and C. Schmitt, Phys. Rev. C **97**, 034319 (2018).

[23] J. Randrup and P. Möller, Phys. Rev. C **88**, 064606 (2013).

[24] A. J. Sierk, Phys. Rev. C **96**, 034603 (2017).

[25] P. Möller and J. Randrup, Phys. Rev. C **91**, 044316 (2015).

[26] P. N. Nadtochy, E. G. Ryabov, A. E. Gegechkori, Y. A. Anischenko, and G. D. Adeev, Phys. Rev. C **89**, 014616 (2014).

[27] R. A. Gherghescu, Phys. Rev. C **67**, 014309 (2003).

[28] R. A. Gherghescu, W. Greiner, and G. Münzenberg, Phys. Rev. C **68**, 054314 (2003).

[29] D. Poenaru, R. Gherghescu, and W. Greiner, Nucl. Phys. A **747**, 182 (2005).

[30] M. T. Senthil Kannan and M. Balasubramaniam, Eur. Phys. J. A **53**, 164 (2017).

[31] R. K. Gupta, M. Balasubramaniam, C. Mazzocchi, M. La Commara, and W. Scheid, Phys. Rev. C **65**, 024601 (2002).

[32] M. Balasubramaniam, R. Kumar, R. K. Gupta, C. Beck, and W. Scheid, J. Phys. G: Nucl. Part. Phys. **29**, 2703 (2003).

[33] R. K. Gupta, R. Kumar, N. K. Dhiman, M. Balasubramaniam, W. Scheid, and C. Beck, Phys. Rev. C **68**, 014610 (2003).

[34] S. S. Malik and R. K. Gupta, Phys. Rev. C **39**, 1992 (1989).

[35] R. K. Gupta, W. Scheid, and W. Greiner, J. Phys. G: Nucl. Part. Phys. **17**, 1731 (1991).

[36] S. Kumar and R. K. Gupta, Phys. Rev. C **49**, 1922 (1994).

[37] W. Greiner and R. K. Gupta, *Heavy Elements and Related New Phenomena* (World Scientific, Singapore, 1999), https://www.worldscientific.com/doi/pdf/10.1142/3664.

[38] J. Maruhn and W. Greiner, Phys. Rev. Lett. **32**, 548 (1974).

[39] R. K. Gupta, W. Scheid, and W. Greiner, Phys. Rev. Lett. **35**, 353 (1975).

[40] D. R. Saroha and R. K. Gupta, J. Phys. G: Nucl. Phys. **12**, 1265 (1986).

[41] J. A. Maruhn and W. Greiner, Phys. Rev. C **13**, 2404 (1976).

[42] H. Kroger and W. Scheid, J. Phys. G: Nucl. Phys. **6**, L85 (1980).

[43] K. L. Couteur and D. Lang, Nucl. Phys. **13**, 32 (1959).

[44] H. A. Bethe, Rev. Mod. Phys. **9**, 69 (1937).

[45] H. J. Krappe, Phys. Rev. C **59**, 2640 (1999).

[46] W. D. Myers and W. J. Swiatecki, Nucl. Phys. **81**, 1 (1966).

[47] J. Blocki, J. Randrup, W. Swiatecki, and C. Tsang, Ann. Phys. **105**, 427 (1977).

[48] R. K. Gupta, D. Singh, R. Kumar, and W. Greiner, J. Phys. G: Nucl. Part. Phys. **36**, 075104 (2009).

[49] C. Karthikraj and M. Balasubramaniam, Phys. Rev. C **87**, 024608 (2013).

[50] C. Simenel and A. S. Umar, Phys. Rev. C **89**, 031601(R) (2014).

[51] D. Regnier, N. Dubray, N. Schunck, and M. Verrière, Phys. Rev. C **93**, 054611 (2016).

[52] T. R. England and B. F. Rider, Evaluation and compilation of fission product yields 1993, Technical Report No. LA-SUB-94-170, Los Alamos National Laboratory, NM, United States (1995).

[53] B. D. Wilkins, E. P. Steinberg, and R. R. Chasman, Phys. Rev. C **14**, 1832 (1976).